Polyelectrolyte self-assembly on polymeric nanofiltration substrates: insight into thin film growth and surface modification

Machawe M. Motsa[a,*], Bhekie B. Mamba[a,b]

[a]*Nanotechnology and Water Sustainability (NanoWS) Research Unit, School of Science, Engineering and Technology, University of South Africa, Florida Campus, P.O. Box: 392, Pretoria 003, South Africa, Tel. +27 11 670 9480; emails: motsamm@unisa.ac.za (M.M. Motsa), mambamm@unisa.ac.za (B.B. Mamba)*
[b]*State Key Laboratory of Separation and Membrane Processes, National Centre for International Joint Research on Separation Membranes, School of Materials Science Engineering, Tianjin Polytechnic University, Tianjin 300387, P.R. China*

ABSTRACT

This study discusses the preparation and characterization of polyelectrolyte multilayers deposited on polyacrylonitrile (Pan) and polyethersulfone (Pes) polymer substrates. Emphasis was made on investigating the polyelectrolyte thin film development and the effect of polycation–polyanion combination on bi-layer structural configuration. The membranes performance indicators (water permeability and salt rejection) were determined through laboratory tests. Membrane surfaces were extensively studied with spectroscopic (Fourier transform infrared and X-ray photoelectron spectroscopy) techniques and electrokinetic analysis as well as wettability measurements. It was revealed that subsequent deposition of PEI/PSS or PAH/PSS multilayers resulted in the emergence of new membrane functionality. The Pan substrate was easily modified and allowed the adsorption of polyelectrolyte multilayers due to the presence of amine groups that interacted with the ionized polyions. The ultrathin polyelectrolyte films resulted in favorable interactions between the membrane and water molecules which was due to the increased polar component of the membrane surface free energy. The modified substrates were then tested for their separation properties and they exhibited a good rejection (>85%) for salts of multivalent cations ($MgSO_4$ and $CaCl_2$) and an average removal for NaCl and KCl. Salt removal followed this order $MgSO_4 > CaCl_2 > NaCl \geq KCl$ for all the membranes types. The eventual ion removal was a function of the combined actions of electrostatic and acid-base forces as well as the membrane sieving effect.

Keywords: Brackish water; Desalination; Interactions; Membranes; Polyelectrolytes; Salt rejection; Substrates

1. Introduction

The purification of wastewater and ground water using membrane processes has emerged as a promising long-term and sustainable alternative to supplement the fading natural water sources [1,2]. However, these water streams, particularly wastewater; is characterized by the presence of organic, inorganic compounds, dissolved macromolecules and bacterial cultures that are responsible for membrane fouling during filtration. Fouling has adverse effects on membrane performance and permeate quality [3–6]. Brackish and ground water on the other hand constitute of a high content of mineral ions such as Na$^+$, K$^+$, Ba^{2+}, Ca^{2+} and Mg^{2+} amongst other substances. Effective removal of these ionic species usually requires the use of pressure driven reverse osmosis processes [7]. However, one over-emphasized drawback of the reverse osmosis process is its heavy reliance on external hydraulic pressured which leads to high energy consumption

* Corresponding author.

of the overall water treatment process. [8]. Nanofiltration (NF) processes require lesser external driving force compared with reverse osmosis, but it has average removal of divalent salts and low retention of monovalent salts [9]. Therefore, surface modification of basic nanofiltration membranes presents an opportunity to prepare high performance NF membranes with high water flux and good selectivity for cationic species. One way of modifying membrane surface is enhancing its surface hydrophilicity [10,11].

Surface modification ranges from the addition of certain surface functional groups to the incorporation of nanoparticles that possesses anti-fouling properties [12–14]. Electrostatic self-assembly (ESA) is one of the methods that can also be utilized to alter membrane surface properties. It is an inherently simple, robust technique that involves the sequential deposition of oppositely charged polyelectrolytes resulting in the formation of ultrathin membrane films with controlled thickness [15–17]. The formed multilayers introduce different functionality onto the membrane surface thus modifying its surface interfacial properties. This process is also referred to as layer-by-layer (LBL) assembly method; thus, the acronyms ESA and LBL will be used interchangeably throughout the text [18,19]. The driving force in an ESA deposition is the electrostatic attraction force between the oppositely charged polyelectrolytes [20,21].

The immanent advantages of the LBL method include being a simple operation, and in most cases, water is the only solvent used to dissolve polyelectrolytes; thus, reducing the consumption of harmful solvents. Additionally, the deposited polyelectrolyte layer also possesses antifouling property against organic foulants because of its hydrophilicity [10,22–24]. It is for these reasons that the process has attracted much attention recently in the preparation of NF membranes [25,26].

The incorporation of nanoparticles (inorganic materials) into the LBL method was explored by several researchers. Lui et al, [27] prepared a novel nanocomposite NF and forward osmosis membranes with improved antibacterial properties by embedding silver nanoparticles into ESA assembled layers. Saren et al, [28] used the LBL technique to prepare NF-like FO membranes with good retention for magnesium chloride. Hu and Mi [29] fabricated a novel water purification membrane through LBL assembling of negatively charged graphene oxide (GO) nanosheets on a porous poly(acrylonitrile) support and interconnecting them with positively charged poly(allyamine hydrochloride) (PAH) aimed for forward osmosis purposes. They demonstrated that bilayers (GO-PAH) were dominated by GO due to its higher mass. The resulting membrane showed improved water permeability and ion rejection. In another work, Kang et al, [30] incorporated zeolite nanoparticles into poly(acrylonitrile) based nanocomposite membrane to improve water permeability. The zeolitic material was sandwiched between a polyelectrolyte pair of poly (acrylic acid) and polyethylenimine (PEI). The incorporation of zeolite nanoparticles was found to enhance membrane water permeability without compromising membrane selectivity for tested species.

The LBL method was also used by Karmer et al. [31], to modify commercial polyethersulfone membranes by successively adsorbing chitosan and alginate to enhance anti-biofouling properties. And fouling tests with model organic foulant (alginate) and *Escherichia coli* revealed that the deposited layers improved resistance to biological fouling and water permeability. The inert graphene oxide nanosheets were also used to coat a polyamide membrane in a bid to improve its stability against chlorine corrosion. Consequently, it was demonstrated that the conformal GO coating layers increased the surface hydrophilicity and reduced surface roughness, leading to significantly improved antifouling performances against protein foulant [32]. In a recent study by IIyas et al. [33], an ultrafiltration membrane was successfully modified by sequential deposition of PAH and PAA multilayers that acted as sacrificial layers to allow easy cleaning of membranes. In a different work by Zhang et al, [34] bilayers of PEI and PAA were deposited on poly(acrylonitrile) substrates for pervaporation separation of water/alcohol mixtures.

Inspired by previous studies, this work intended to prepare high flux LBL membranes with improved rejection for cationic species aimed for treating brackish water. Developing understanding of the mechanisms of polyelectrolyte multilayer formation and the role of various substrates in film growth and multilayer interfacial properties is fundamental for their application in water purification processes. Therefore, polyelectrolyte multilayers still require extensive investigation in accordance to their stability and response to various external conditions.

This work used PEI, PAH and PSS to develop selective ultrathin multilayers on poly(acrylonitrile) and polyethersulfone nanofiltration substrates. Emphasis was focused on the interaction between polymeric substrates and the polyelectrolytes. Multilayer formation was monitored using various techniques such as atomic force microscopy (AFM), Fourier transform infrared (FTIR), electrokinetic analyzer, drop shape analyzer and X-ray photoelectron spectroscopy (XPS). The influence of membrane surface functionality on water permeability and ion rejection was studied. The produced membranes were then compared with the commercially available nanofiltration membrane (NF90).

2. Experimental

2.1. Materials

All the chemicals used in this study were used as received without further purification. Polyacrylonitrile (Pan) weight averaged molecular weight Mw ≈ 150,000 (Sigma-Aldrich, Johannesburg, South Africa) and polyethersulfone were used as polymers (Solvay). N,N-dimethylformamide (DMF, 99.8%), and lithium chloride were used as the solvent, and pore former, respectively, for the fabrication of the membrane substrates. Sodium hydroxide (Sigma-Aldrich, Johannesburg, South Africa) was used as the alkali solution for the post-treatment of Pan/Pes membrane substrates to enhance its surface charge density and hydrophilicity. Polyethylenimine (branched PEI, Mw ≈ 15,000), poly(allylamine hydrochloride) (PAH, Mw ≈17,500) and poly(sodium 4 styrene-sulfonate) (PSS, Mw ≈ 20,000; Fig. 1) were also obtained from Sigma-Aldrich (Johannesburg, South Africa) and were used as the respective polycation and polyanion for LBL assembly. Sodium chloride (Sigma-Aldrich,

Poly(acrylonitrile)   *Poly(ether sulfone)*   *Poly(allylamine hydrochloride)*

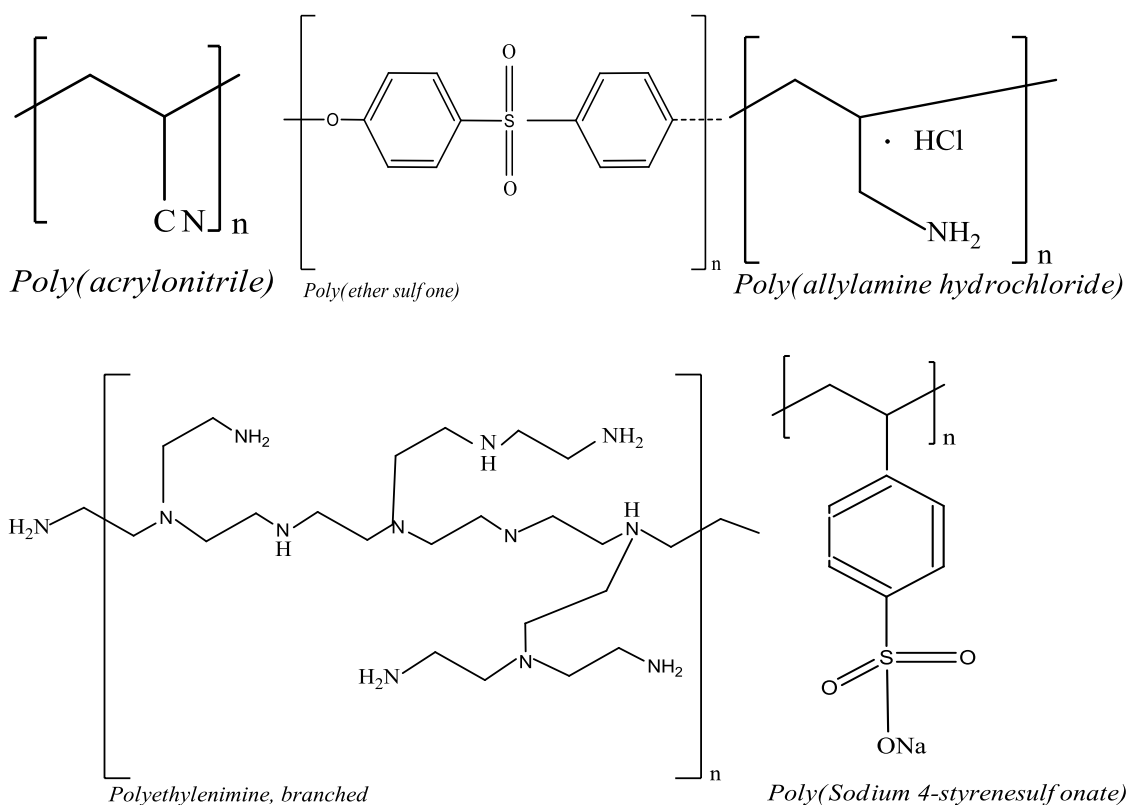*Polyethylenimine, branched*   *Poly(Sodium 4-styrenesulfonate)*

Fig. 1. Structural formulas of used polymers (Pan and Pes) and polyelectrolytes (PAH, PEI and PSS).

Johannesburg, South Africa) was used to adjust the ionic strength of the polyelectrolyte solutions during LBL assembly. Membrane solute rejection properties were determined using four solutions containing calcium chloride, magnesium chloride, potassium chloride, and sodium chloride (Sigma-Aldrich, Johannesburg, South Africa). The short forms: Pan and Pes were used to represent poly(acrylonitrile) and polyethersulfone throughout the manuscript.

2.2. Substrate preparation

The polymers (Pan, Pes: 18 wt.%) and LiCl (2 wt.%) were dissolved in DMF in a sealed container at 60°C. To achieve complete dissolution, the solution was stirred for at least 24 h. The polymer solution was then allowed to cool to room temperature before use [35]. A casting knife was used to spread the polymer solution onto a polyester non-woven fabric obtained from Hirose Paper Manufacturing Co. Ltd., Kochi, Japan, which was attached onto a clean glass plate by an adhesive tape. The casting knife gate height was fixed at 150 μm. The glass plate was then immersed into a coagulant bath containing deionized water at room temperature. The nascent substrate was washed with deionized water for 5 min to remove excess solvent.

2.3. Layer by layer assembly/polyelectrolyte self-assembly

The resulting Pan/Pes substrate was soaked in 1.5 M NaOH at 45°C for 1.5 h; the purpose of the NaOH treatment

was to introduce negative charges on the substrate via partial hydrolysis, which is important for the subsequent deposition of counter polyelectrolytes. The alkali treatment was followed by thorough rinsing with deionized water, at which point it was then transferred to PEI and PSS solutions for LBL treatment. Polyelectrolyte solutions were prepared by dissolving 1 g/L of PEI, PAH and PSS in 0.5 M NaCl solution. The polyelectrolyte thin skin on the top surface was formed by soaking the substrate in (but only exposing its top surface) the PEI/PAH solution and then the PSS solution. Each polyelectrolyte soaking step lasted for 45 min, followed by a 3-min deionized water rinsing to remove the excess polyelectrolytes. The above PEI/PSS or PAH/PSS deposition procedure was repeated to form multiple polyelectrolyte layers. Finally, the electrostatically assembled layers were chemically cross linked by immersing the membranes into a 0.1 wt.% glutaraldehyde solution at pH 2–3 for 2 h [36]. Up to four bi-layers were deposited on Pan and Pes substrates, and since PSS was the only polyanion used it was excluded from the membrane naming; so the prepared membranes were labeled as follows: Pan-PEI (1–4), Pes-PEI (1–4) and Pan-PAH (1–4).

2.4. Membrane characterization

The surface morphologies, cross-sectional configuration and roughness of the synthesized substrates and layered membranes were studied using an atomic force microscope (AFM: Alpha300, Germany) and scanning electron

microscope (SEM, JEOL IT300, Tokyo, Japan). Small representative pieces of the membrane samples were dried overnight, then coated with carbon prior to analysis with the microscope. Attenuated total reflectance Fourier transform infrared spectroscopy (ATR-FTIR) was employed to determine the functional groups on the membrane surface (FTIR Spectrometer, PerkinElmer, Germany). XPS analysis was performed on an AXIS SupraTM by Kratos Analytical Limited (UK) with a monochromatic Mg Kα X-ray as the excitation source. Binding energy was calibrated with respect to the signal from adventitious C 1s binding energy at 284.8 eV. This was done to study the elemental composition of the membrane surface functionality.

Streaming potential measurements were carried out with a SurPASS Electrokinetic Analyzer (Anton Paar GmbH, Austria) to evaluate membrane surface charge. Measurements were carried out with 0.01 mol/L KCl aqueous solutions at 23°C at a pH of about 6.12. Surface zeta potentials were determined from the measured streaming potentials according to the Helmholtz–Smoluchowski equation (Eq. (1)). The data presented were average values from three samples of each membrane type.

$$\zeta = \frac{\Delta V \cdot \eta \cdot \sigma}{\Delta P \cdot \varepsilon \cdot \varepsilon_0} \tag{1}$$

where ΔV is the measured streaming potential, η is the electrolyte viscosity (Pa.s), electrolyte's electrical conductivity (s/m), ΔP is the applied pressure and ε is the permittivity of water (C^2 N^{-1} m^{-2}). The permittivity is defined as $\varepsilon = \varepsilon_0 D$, where ε_0 is permittivity of vacuum = 8.85×10^{-12} (C^2 N^{-1} m^{-2}) and D is the dielectric constant of water = 78.55 at 25°C.

Contact angle (θ) measurements are generally used to determine the surface free energy through the Young–Dupre equation (Eq. (2)) which links the contact angle of a drop of a liquid placed on a flat solid surface with the surface tension of a liquid, according to van Oss [37].

$$\gamma_l (1 + \cos\theta) = 2\left(\sqrt{\gamma_s^{LW}\gamma_l^{LW}} + \sqrt{\gamma_s^+\gamma_l^-} + \sqrt{\gamma_s^-\gamma_l^+}\right) \tag{2}$$

where θ is the measured contact angle; γ^{LW} is the Lifshitz–van der Waals free energy component; γ^+ is the electron-acceptor component; γ^- is the electron donor component; and the subscripts "s" and "l" designate the solid and liquid phases, respectively. The left-hand side of the equation represents the free energy of cohesion per unit area of the liquid (l) and the right hand side represents the free energy of adhesion per unit area between the liquid (l) and the solid (s) [38,39].

The boundary between hydrophobicity and hydrophilicity occurs when the difference between the apolar attraction and the polar repulsion between molecules or particles of material (s) immersed in water (l) is equal to the cohesive polar attraction between the water molecules [37]. The surface free energy per unit area ΔG_{SWS}^{TOT} (mJ/m²) at contact between similar solid materials (s) gives an indication of the attraction and repulsion between the two interfaces when immersed in liquid medium (w) [38,40]. The total surface free energy of adhesion was determined from the Lifshitz–van der Waals and the acid-base components according to:

$$\Delta G_{SWS}^{TOT} = \Delta G_{SWS}^{LW} + \Delta G_{SWS}^{AB} \tag{3}$$

$$\Delta G_{SWS}^{LW} = 2\left(\sqrt{\gamma_w^{LW}} - \sqrt{\gamma_s^{LW}}\right)\left(\sqrt{\gamma_s^{LW}} - \sqrt{\gamma_w^{LW}}\right) \tag{4}$$

$$\Delta G_{SWS}^{AB} = 2\sqrt{\gamma_W^+}\left(\sqrt{\gamma_S^-} + \sqrt{\gamma_S^-} - \sqrt{\gamma_W^-}\right) + 2\sqrt{\gamma_S^-}\left(\sqrt{\gamma_S^+} + \sqrt{\gamma_S^+} - \sqrt{\gamma_W^+}\right) - 2\sqrt{\gamma_S^+\gamma_S^-} - 2\sqrt{\gamma_S^-\gamma_S^+} \tag{5}$$

Surface free energy components of a membrane can be determined by measuring contact angles between the membrane and three well-characterized probe liquids with known surface tension components, such as deionized water, glycerol and diiodomethane. The tension components of these three liquids are listed in Table 1. The sessile drop method was used to measure the contact angles of the probe liquids (4 μL droplet) employing a Kruss Drop Shape Analyzer, DSA30 (KRUSS GmbH, German) on dried surfaces of the membranes at about 24.0°C using a 5.0 μL syringe. The contact angles were captured from a digital video image of the drop on the membrane. At least 10 measurements on different locations of the membrane sample were performed and averaged to obtain the contact angle of the measured membrane sample.

2.5. Determination of membrane separation parameters

Pure water permeability and salt rejection of the prepared membranes were evaluated in a laboratory-scale crossflow pressure-driven test unit. The effective membrane area (A) was 41.86 cm², the applied pressure (ΔP) ranged from 3 to 15 bar at a constant water temperature of 23.1°C. The loaded membrane sample was first compacted with deionized water at pressure above the operational pressure for at least 3 h, until the permeate flux reached a steady state. The feed volume was fixed at 10 L.

Pure water flux, J_W, was calculated from the total amount of the collected permeate (V) for a fixed time (t) per surface area (A) as expressed by Eq. (6).

$$J_W = \frac{V}{At} \tag{6}$$

The intrinsic water permeability, A, was calculated by dividing the water flux by the applied hydraulic pressure as described in Eq. (7).

$$A = \frac{J_W}{\Delta P} \tag{7}$$

Table 1
Surface tension components (mJ/m²) of probe liquids

Probe liquid	γ^{LW}	γ^+	γ^-	γ^{AB}	γ^{TOT}
Water	21.8	25.5	25.5	51.0	72.8
Glycerol	34.0	3.9	57.4	30.0	64.0
Diiodomethane	50.8	0.0	0.0	0.0	50.8

The observed salt rejection (R) was determined from the difference in bulk feed (C_b) and permeate (C_p) salt concentrations (Eq. (8)). The applied pressure was kept at 7 bars, permeate samples of 250 mL were collected and a calibrated conductivity meter was used to measure their electrical conductivity.

$$R = 1 - \frac{C_p}{C_b} \qquad (8)$$

The calculated salt rejection (R) was then used to compute the membranes' solute permeability coefficient, B, using Eq. (9).

$$B = \left(\frac{1}{R} - 1\right) \times A(\Delta P - \Delta \pi) \qquad (9)$$

where $\Delta\pi$ is the osmotic pressure of the feed solution, given by Eq. (10).

$$\pi = imRT \qquad (10)$$

where i is the van't Hoff coefficient, m is the molarity of the solution, R is the universal gas constant and T is the absolute temperature.

The salt flux, J_S across the membrane was calculated using Eq. (11).

$$J_s = J_W \frac{B}{AiRT} \qquad (11)$$

3. Results and discussion

3.1. Membrane surface morphology and roughness

The surface image (Fig. 2a) is characterized by a rough ridged-like surface belonging to the hydrolyzed Pan substrate. The ridged-like (rough-cast) appearance disappeared when three and four polyelectrolyte bilayers were deposited resulting in a neat layered surface as shown by Figs. 2b and c. The changes in surface morphology of the substrate confirm the successful deposition of the polyelectrolyte layers. The cross-sectional image (Fig. 2d) is exhibiting an asymmetric configuration consisting of an ultrathin skin
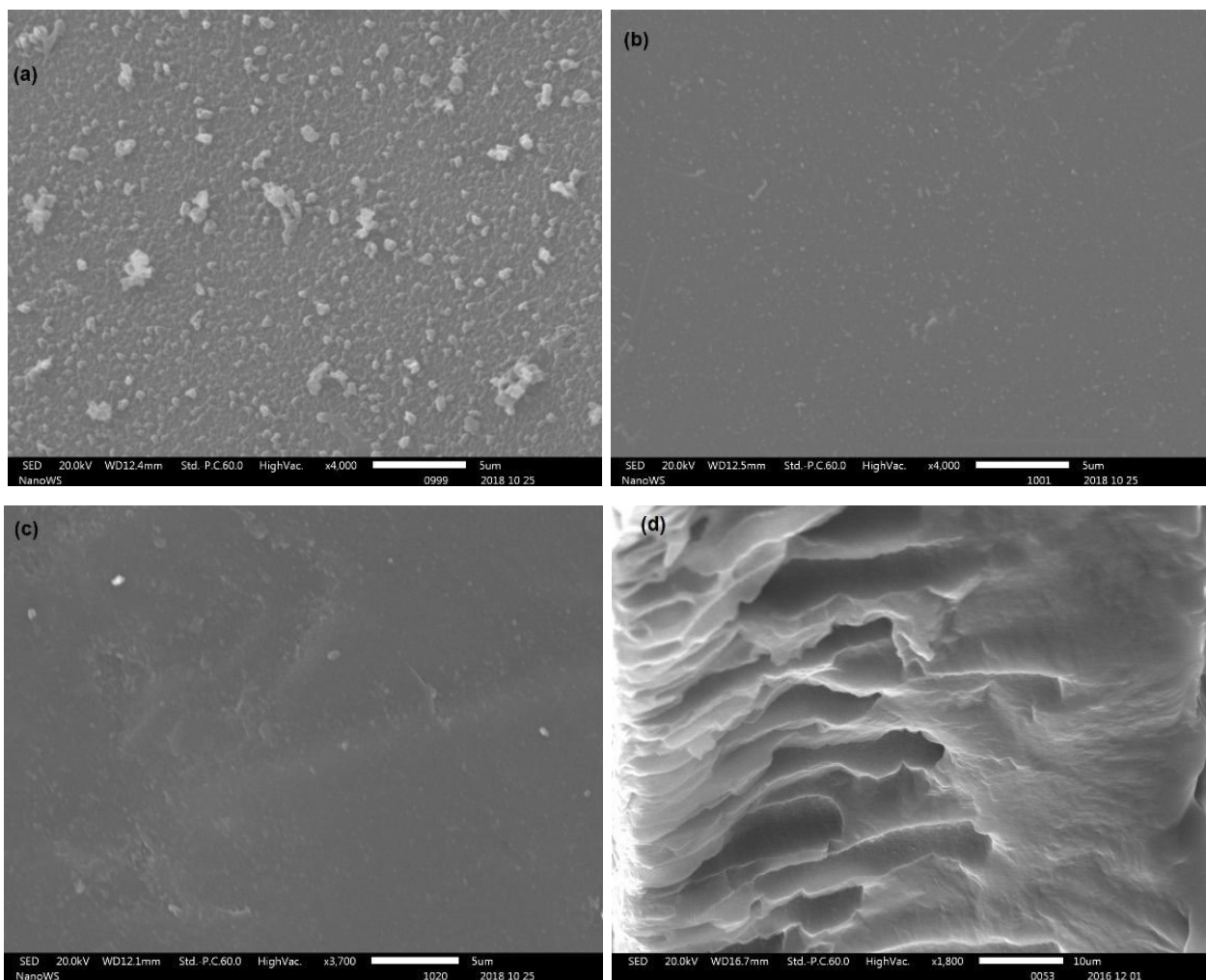

Fig. 2. SEM micrographs of the prepared layer-by-layer assembly membranes: Surface view of (a) unmodified Pan substrate, (b) Pan-PAH-3, (c) Pan-PAH-4 and (d) the cross-sectional view of the membranes.

layer followed by finger-like macro-voids resulting from solvent-non-solvent de-mixing during phase inversion. This layer is terminated by a dense, compact layer at the bottom of the membrane.

The deposition of the ultrathin polyelectrolyte multilayers on the surface was further investigated by performing a scratch test using AFM cantilever. The scratched part was then analyzed using a non-contact mode and SEM to result in the images in Figs. 3a and b. Parts of the layers were peeled-off the surface due to the scratch exerted by the cantilever and are visible on the SEM image revealing a layered structure. The resulting surface topology (Fig. 3a) shows a ridge and valley (a corrugated configuration) further confirming the layered structure.

The roughness of the prepared LBL membranes showed no clear correlation between surface roughness and number of bi-layers for the three sets of membranes. However, the overall observation was that surface roughness slightly increased with the number of bilayers for the Pan-PEI and

Pan-PAH membranes. The surface roughness for the Pan-PEI and Pan-PAH membranes were low, which suggest that the multilayers resulting from the Pan-PEI/PSS and PAH/PSS pairs are more aligned and compact resulting in smoother morphology compared with the Pes-PEI/PSS membranes.

3.2. Membrane zeta potential and FTIR analysis

The development of thin multi-layered films on the membranes was studied using FTIR spectroscopy. Fig. 4a shows the spectra of Pan, PEI, PAH and PSS depicting characteristic peaks across the infrared region. Fig. 4b shows the spectra of the Pan-PEI membranes. There is a clear presence of new functionality as a result of polyelectrolyte coating shown by the presence of the broad peak at $3,307.1$ cm^{-1} which is attributed to alkynes; Sp, C–H stretching which emanates from the presence of both PEI and PSS. There is also the presence of a medium C=N stretching at $1,674.7$ cm^{-1}, a functionality brought by the presence of PEI
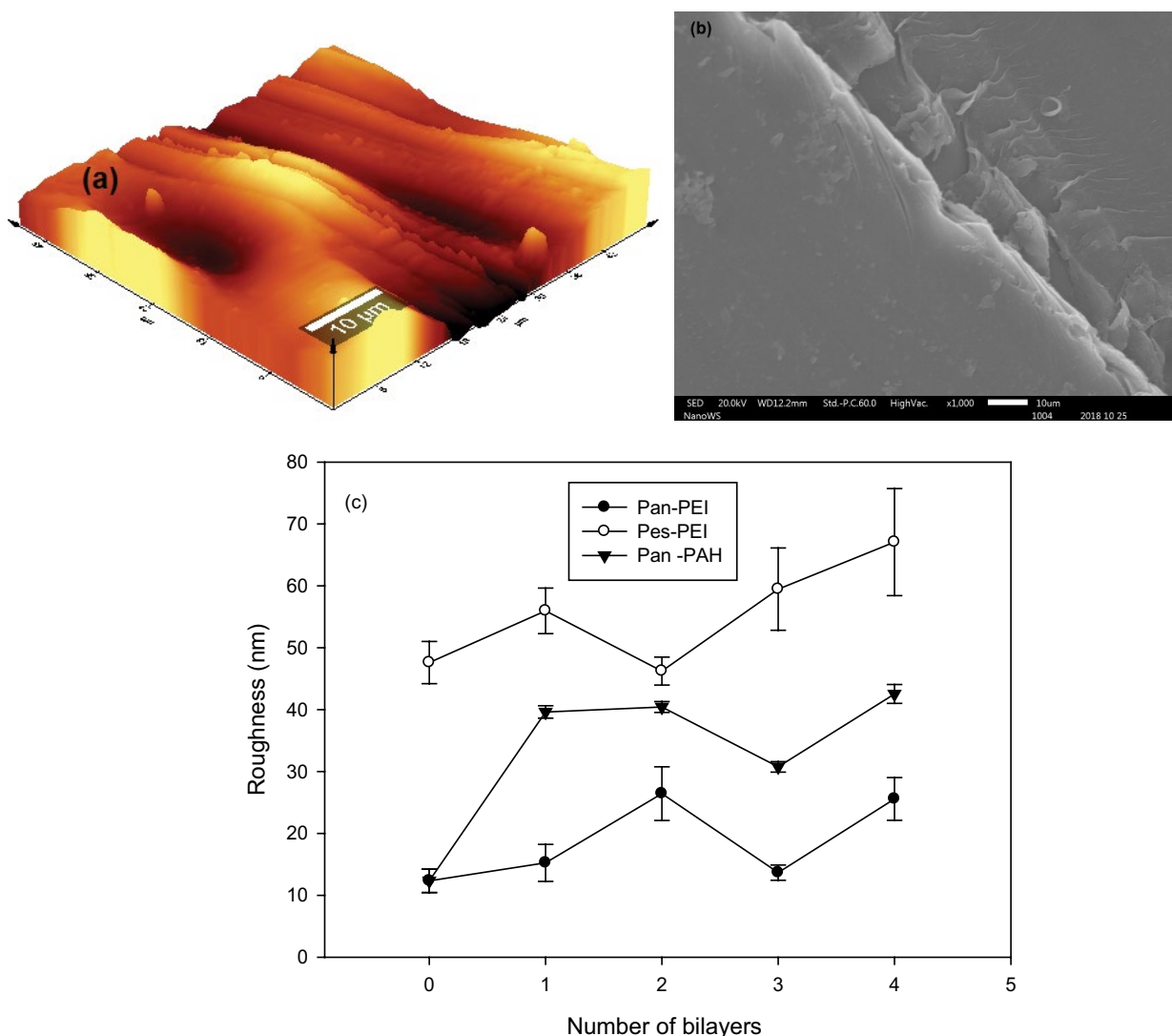

Fig. 3. (a) Surface topology and (b) morphology of the scratched surface as analyzed by AFM and SEM and (c) membrane surface roughness as a function of the deposited bi-layers.

layer. The appearance of a weak peak at 1,215 cm^{-1} reveal the presence of a C=C stretch, which confirms the presence of polyelectrolyte chains on the membrane surface.

Fig. 4c shows the spectra of PES-based LBL membranes, there is no strong evidence of surface modification from the presented spectra except for the presence of weak peaks at 1,035.28 cm^{-1} for the 3rd and 4th layers which is assigned to alkoxy groups (C–O) that have arose from the cross-linking amongst the layers. There is also a weak peak at 1,640 cm^{-1} which corresponds to C=N stretching and C=C aromatic stretching from the PSS. Meanwhile Fig. 4d displays the spectra of the Pan-PAH layered membranes, presenting a strong indication of surface modification with clear peaks at the 3,300 cm^{-1} region which corresponds to the Sp C–H stretching, primary and secondary amine (N–H) stretching contributed by the PEI and PSS. The 1,553.86 cm^{-1} peak was a result of a C=C stretching from the aromatic ring of PSS. There was also a shift of the C=C alkene stretching and N–H bending peaks at 1,624 to 1,660 cm^{-1}. As well as the shift of the Sp^3 C–H bend from 1,369 to 1,395 cm^{-1}. Peak at 1,560 cm^{-1} corresponds to the COONa stretching. The presence of –SO$_3^-$ group of the PSS polyelectrolyte at 1,006; 1,035 and 1,126 cm^{-1} and –CH=N– group of the PAH polyelectrolyte at 1,627 cm^{-1}. There was also the emergence of the weak peak at the 1,220–1,202 cm^{-1} region due C–O functionality. The FTIR spectra revealed that the membrane surfaces were modified

by the deposition of PEI/PSS and PAH/PSS bilayers. The infrared spectroscopy spectra were further supported by the UV-Vis analysis (Fig. A1(a)), which displayed a change in the absorbance intensity. This was an indication of the modification/rearrangement in the structure of the UV excitable functional groups as a result of the interaction between the polyacrylonitrile chain and the polyelectrolytes.

The surface of the Pan-PEI membranes was further characterized with XPS to study its elemental composition. Figs. 5a and b show the wide XPS scans for the Pan, Pan-PEI_1 and Pan-PEI_4 membranes. They show strong peaks that are attributed to C1s, N1s and O1s at various binding energies as listed in Table 2. There is also peak attributed to the presence of Na$^+$ which emanates from the presence of the poly(sodium 4-styrenesulfonate) layers on the membrane surface.

The nitrogen content of the poly(acrylonitrile) substrate was significantly reduced upon deposition of the PEI and PSS polyelectrolytes, furthermore, it slightly increased from 6.51% to 7.14% after four polyelectrolyte bi-layers. The Pan-PEI_1 and Pan-PEI_4 membranes showed a significant presence of oxygen (O1s) with a concentration of about 17%. Further resolution of the XPS scan peaks showed the presence of new bonds in the structure of the polyelectrolyte films as shown in Figs. 5c–j and they were assigned as listed in Table 2. The bonds assigned in Pan-PEI_1 were repeated in
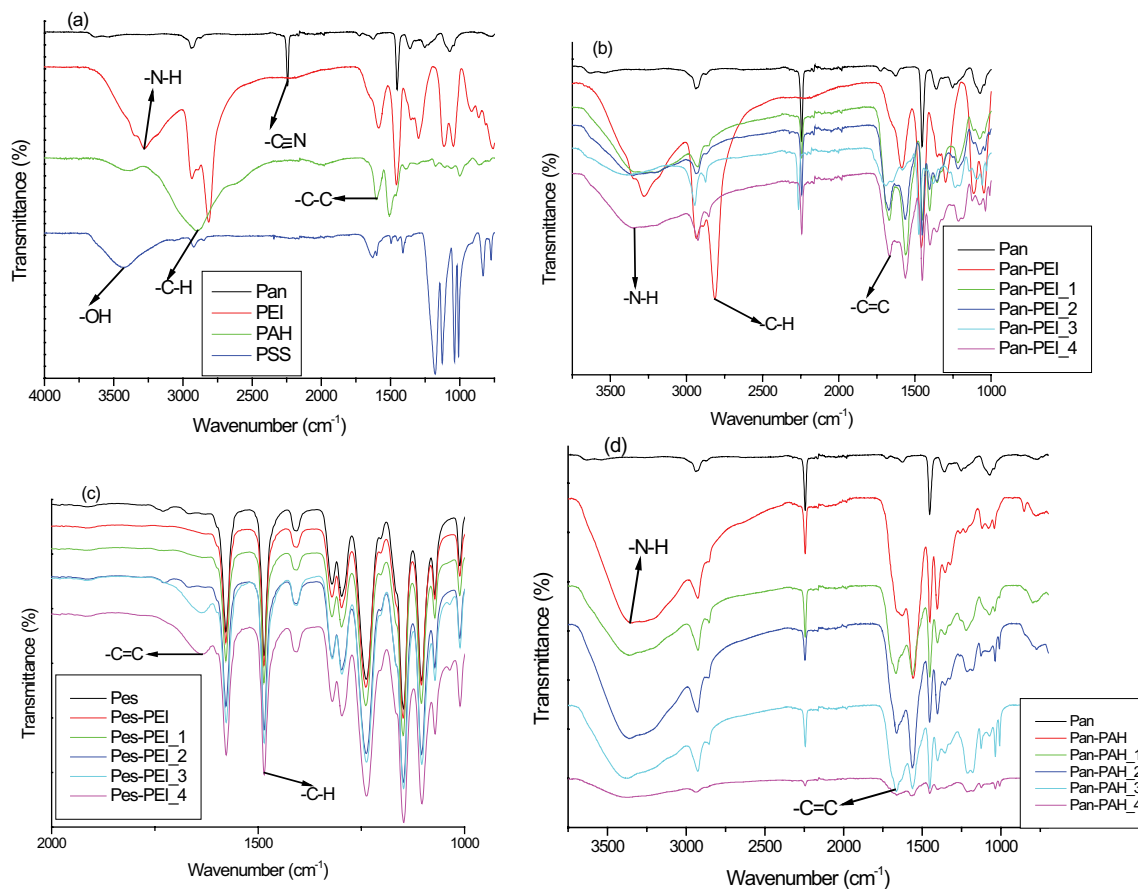

Fig. 4. Infrared spectra of prepared membranes: (a) spectra of polymer and polyelectrolytes, (b) spectra of Pan-PEI membranes, (c) spectra of Pes-PEI membranes and (d) spectra of Pan-PAH membranes.
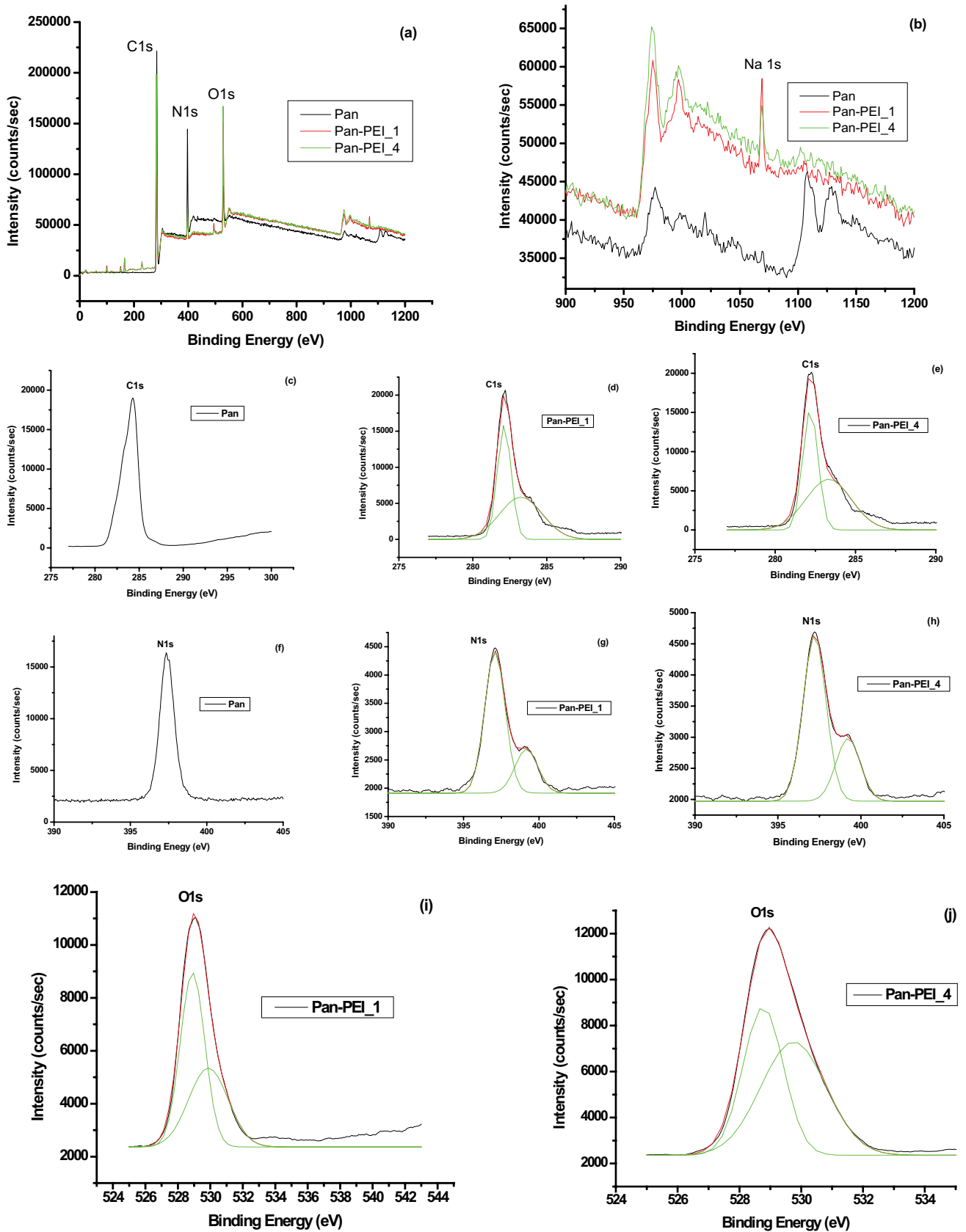
Fig. 5. XPS spectra of the PEI-PSS bi-layers on the Pan polymer substrate. (e) C1s - Pan, (d) C1s – Pan-PEI_1, (e) C1s - Pan-PEI_4, (f) N1s – Pan, (g) N1s - Pan-PEI_1, (h) N - Pan_PEI_4, (i) O - Pan-PEI_1, and (j) O – Pan-PEI_4.

Table 2
Surface elemental composition of prepared membranes after XPS analysis

Membrane sample	Elements	Atomic concentration (%)	Binding energy (eV)	Assignment
Pan	C	76.03	284.4	–C–H
	N	18.55	397.3	–C–N
Pan-PEI_1	C	76.93	282.1 (56.2%)	–C=C–
			283.3 (20.7%)	–C–C–
	N	6.51	397.1 (4.97%)	–C–N
			399.2 (1.54%)	–N–H
	O	16.56	529.9 (5.16%)	–O–Na
			528.9 (11.40%)	–O=O–
	Na		1,071.6.8	–O–Na
	S		168.2	–S–O

Pan-PEI_4 in similar binding energies, with slight variations in their concentrations which is attributed to the increased presence of polyelectrolyte layers. The detected functional groups (elemental bonds) suggest the superior presence of the PSS polyelectrolyte which is understandable since all multilayers were terminated by the negatively charged poly(4-Sodium styrenesulfonate). These spectroscopic results revealed that the poly(acrylonitrile) base was easily modified by coating with polyelectrolyte layers, mainly due to the presence of nitrogen-based functionality on its surface that can act as electrophiles and form bonds with the polycations (PEI and PAH) which also contain amine groups.

Zeta potential measurements were used to monitor the changes in surface charge as a function of polyelectrolyte deposition on the treated substrate surface (Fig. 6a). The treated substrate surface exhibited a very negative charge because of the partial hydrolysis resulting from NaOH treatment. Deposition of the positively charged PAH transitioned the surface charge into positive values. The PAH adsorption was followed by PSS deposition as per the procedure during LBL assembly. This resulted in a sharp decrease and eventual reversal of the highly positive surface to a strong negative charge. This experiment is proof of the strong attractive electrostatic forces between the oppositely charged polyelectrolytes during self-assembly, thus; giving insight into the growth of these polyelectrolyte multilayers on the substrate.

The surface charge of the prepared LBL membranes was determined to give the pattern shown by Fig. 6b, which is highlighted by the relatively poor zig-zag format of the measured zeta potentials. The deposition of the cationic PEI and PAH changed the negatively charged Pan and Pes surfaces into positive charge, with PAH contributing the highest positive charge (+73 mV) compared with the weakly positive surfaces resulting from PEI deposition. However, the deposition of the negatively charged PSS on surfaces terminated by the cationic PEI/PAH layer reduced the surface charges; the Pan-PAH surface charge was reduced from 73.2 to 35.1 mV. The Pes-based membranes were negative, with Pes-PEI_1 and 4 exhibiting a charge almost similar to that of the plain Pes (–28.5 and –37.2). However, Pes-PEI_2 and 3 recorded weak negative zeta potentials of –4.01 and –1.01, respectively. The Pan-PEI membranes fluctuated between
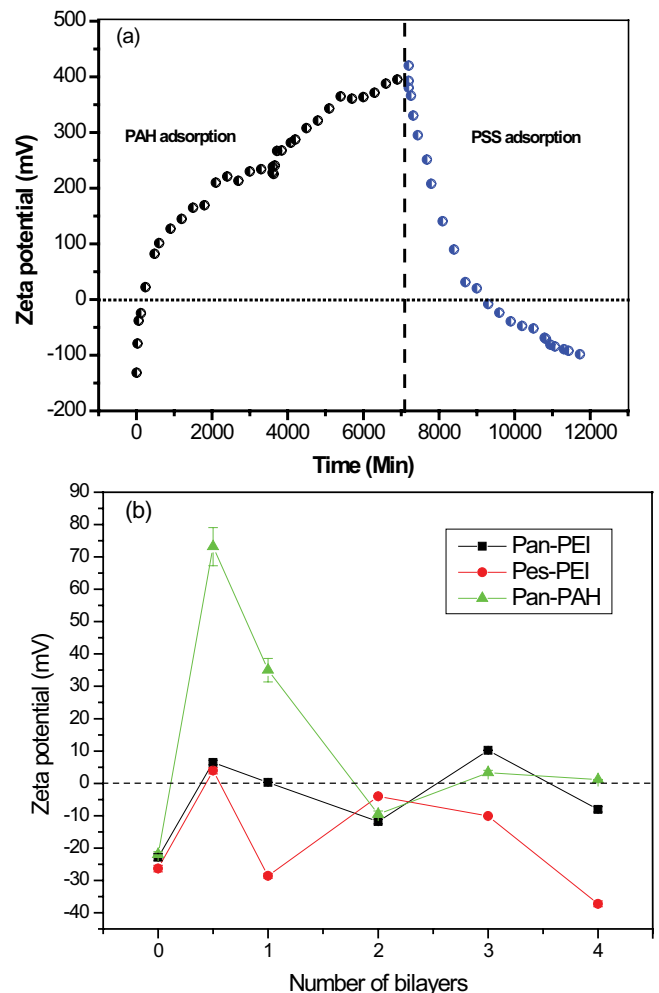

Fig. 6. (a) Adsorption of polyelectrolytes on treated substrate and (b) surface charges of prepared layer-by-layer membranes determined through streaming potential measurements.

negative charges depending on the ratio of the PEI and PSS on the surface. PEI had more influence on the first and third bi-layer, while the negative charge was more pronounced on the second and fourth bi-layers.

The Pan-PAH membranes were relatively positive, with the only deviation presented by the second bi-layer which recorded a weak negative charge (–9.5 mV). The third and fourth bilayers exhibited a weakly positive reading of 3.4 and 1.1 mV. These results further support our aforementioned observations that the surface of the substrates was modified by the electrostatic deposition of counter polyelectrolytes, as earlier reported in previous studies [41,42]. It was also revealed that the charge of the deposited film is dependent on the ratio of the PEI/PSS and PAH/PSS pairs. The non-conformity in the displayed charge patterns resulted from the imbalance in charge densities between the two polyelectrolytes as demonstrated by the measured zeta potential in solution. The PEI solution exhibited a weak positive charge (+6.8 mV) while an expected negative charge (–22.8 mV) was obtained for the PSS solution; this gives explanations for the dominant negative surface charge measured on the PEI/PSS multilayers. From the selected pairs of counter polyelectrolytes, it was revealed that the PES polymer produced negatively charged membranes.

3.3. Membrane water contact angle and surface free energy

The determination of surface free energy components of membranes is regarded as fundamental to developing proper understanding of the mechanisms involved during filtration [39,43]. Generally, the measured water contact angle decreased after the deposition of polyelectrolyte layers for all membrane types as shown in Fig. 7. Extreme decline was observed for the Pan-PEI membranes, decreasing from 74° to 29° after the first bi-layer of PEI and PSS. The subsequent three membranes recorded almost constant contact angles averaging at 33°. The polyelectrolytes layers improved the water-membrane affinity mostly due to the presence of charged functionalities caused by misalignment of the polyelectrolyte as shown by the increasing polar component of surface free energy (γ^{AB}), which further suggested that the membrane surface was easily wetted by water. There was also a decline in water contact angle for the Pes-PEI membranes. However, this drop was not as significant after the first bi-layer was deposited, the contact angle only declined by only 3°; from 69° to 66°. A far bigger margin in measured contact angle was recorded after the 2nd and 3rd polyelectrolyte layers. A similar trend was observed for the Pan-PAH membranes. The most conspicuous observation was that the decline in water contact angles was stagnant after the 4th bi-layer for all three sets of membranes. The number of bi-layers no longer had influence on membrane wettability properties.

In general terms, surface hydrophilicity/hydrophobicity has been defined by the value of the measured contact angle; with an angle of less than 90° considered hydrophilic, with 90° and above regarded as hydrophobic. However, the fundamental definition can be derived from the measurement of contact angles using three well characterized liquids representing the apolar and polar components of surface free energy. The computation of these angles results in ΔG_{SWS}^{TOT} which is the total free energy of cohesion and the sign of ΔG_{SWS}^{TOT} defines the nature of the surface and the magnitude of ΔG_{SWS}^{TOT} is used as the quantitative measure of the surface hydrophobicity or hydrophilicity [40]. When $\Delta G_{SWS}^{TOT} < 0$ the
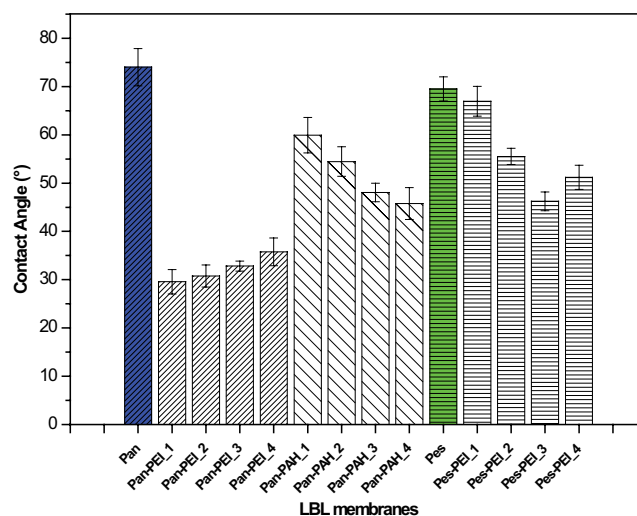

Fig. 7. Measured water contact angles for the three sets of prepared layered membranes.

material is defined as hydrophobic and when $\Delta G_{SWS}^{TOT} > 0$ it is described as hydrophilic.

Table 3 presents the calculated membrane surface free energy components. It shows that all the membranes had a strong electron donor mono-polarity. The Pan and Pan-PEI_1 membranes exhibited a strong single polarity surface that led to a low acid-base (AB) component. However, there was a gradual increase in the electron acceptor polarity when more polyelectrolyte layers were deposited on the membrane surface, which in turn improved its polar component. This was an indication of the contribution of the polyelectrolytes towards the polar component of the membrane surface. The Pan-PEI membranes recorded the lowest contact angles which correlated to its surface polar energy component. A similar observation was made for the Pes-based membranes, Pes and Pes-PEI_1 membranes had a negligible electron acceptor functionality followed by a slight increase upon addition of PEI and PSS bi-layers. The Pan-PAH membranes also followed a similar trend exhibiting relatively low AB component for all four layers.

The values of the surface free energy components correlated with the measured water contact angles. The Pan-PEI membranes had the largest γ^{AB} component supported by the low measured contact angles. The γ^{AB} values for the Pes-PEI and Pan-PAH membranes were almost similar which corresponded to their average water contact angles.

Table 4 presents the total energies of cohesion ΔG_{SWS}^{TOT}, the behavior of similar membrane surfaces when immersed in water. The total Liftshitz–van der Waals energy is always negative which indicates the attractive (hydrophobic) nature of the apolar functionality of the surface. And for most of the prepared membranes, it was smaller than the total acid-base (ΔG_{SWS}^{AB}) energies. According to the calculated total cohesion energies, most of the membranes were hydrophilic (varying degrees of hydrophilicity), except for the plain Pes membrane which recorded a negative energy of cohesion implying that the surface was hydrophobic. The most interesting observation was that the best performing membranes in each set (Pan-PEI_1, Pes-PEI_2 and Pan-PAH_4) exhibited the highest

Table 3
Surface free energy components of prepared layer-by-layer membranes

Membrane	γ^{LW}	γ^+	γ^-	γ^{AB}	γ^{TOT}
Pan	36.72	1E-06	44.16	0.013	36.73
Pan-PEI_1	40.17	1E-06	57.55	0.033	40.19
Pan-PEI_2	33.97	2.31	42.14	19.70	53.71
Pan-PEI_3	33.75	3.74	49.69	27.31	44.45
Pan-PEI_4	38.59	0.25	25.93	5.09	43.70
Pes	39.45	1E-06	18.48	0.0086	39.52
Pes-PEI_1	38.94	1E-06	20.99	0.0092	38.95
Pes-PEI_2	37.88	0.089	28.07	3.16	41.02
Pes-PEI_3	40.41	0.47	31.71	7.72	48.13
Pes-PEI_4	41.76	0.21	26.94	4.76	46.56
Pan-PAH_1	39.19	0.71	33.28	9.72	48.91
Pan-PAH_2	37.68	0.83	23.16	8.77	46.43
Pan-PAH_3	41.16	0.51	28.97	7.69	48.82
Pan-PAH_4	37.96	0.005	42.49	0.92	38.25

Fig. 8. Water permeability of the different prepared membranes layer-by-layer membranes.

Table 4
Free energy of cohesion components for the prepared membranes

Membrane	ΔG_{131}^{LW} (mJ/m²)	ΔG_{131}^{AB} (mJ/m²)	ΔG_{131}^{TOT} (mJ/m²)
Pan	−3.87	32.20	28.40
Pan_PEI_1	−5.57	51.20	45.70
Pan_PEI_2	−2.67	20.40	17.70
Pan_PEI_3	−2.60	24.90	22.30
Pan_PEI_4	−3.80	22.40	18.60
Pes	−9.67	5.80	−3.87
Pes-PEI_1	−7.94	9.46	1.50
Pes-PEI_2	−4.41	4.72	0.31
Pes-PEI_3	−5.70	10.10	4.45
Pes-PEI_4	−4.43	6.58	2.15
Pan-PAH_1	−5.06	12.1	7.04
Pan-PAH_2	−4.32	12.93	8.61
Pan-PAH_3	−6.10	15.77	9.67
Pan-PAH_4	−4.45	29.3	24.80

Fig. 9. Membrane separation performance: solute rejection for $MgSO_4$, $CaCl_2$, NaCl and KCl.

degree of hydrophilicity which correlated with their performance in terms of water permeability when compared with other membranes in the three sets.

3.4. Membrane separation properties

3.4.1. Membrane water permeability and salt rejections

The determined water permeability values for LBL membranes are presented in Fig. 8. Clearly, the deposition of polyelectrolyte bi-layers modified the surface of the Pan and Pes substrates. The basic Pan membrane (substrate) was the most permeable, recording a permeability value (*A*) of 27.7 L m⁻² h⁻¹ bar⁻¹. Deposition of the 1st bi-layer reduced
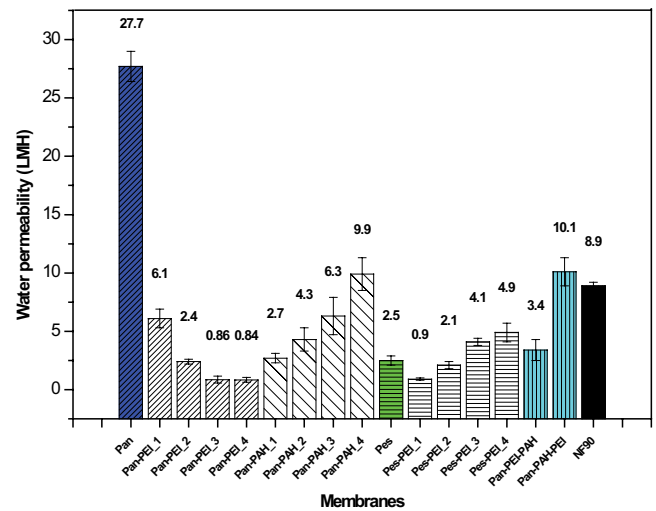
the Pan membrane's permeability by more than three folds to 6.1 L m⁻² h⁻¹ bar⁻¹. The continued deposition of bi-layers further reduced membrane water permeability which is complemented by the improved retention of monovalent cations. The reduction in permeability is attributed to the presence of cross-linked polyelectrolyte layers on the surface that created an extra resistance to water flow.

The PEI/PSS laid Pes membrane had a varying degree of permeability rising from 0.5 to 4.9 L m⁻² h⁻¹ bar⁻¹ which corresponded to the increasing number of bi-layers. The increase in water permeability compromised solute retention. This was a contrasting observation to that made from the Pan-based membranes. The Pes-PEI_2 membrane had the best performance: it had a balanced performance in terms of water permeability and ion rejection. The presence

of polyelectrolyte layers on the surface of Pes-enhanced water transport through the membrane. They improved membrane wettability as supported by the observed contact angle patterns and calculated polar surface free energy components.

The permeability of Pan-PAH membranes was also lower than that of the basic Pan membrane (substrate). However, amongst the prepared LBL membranes; water permeability generally increased with the number of bi-layers (PAH/PSS) which corroborates that the polyelectrolyte pairs improved water permeability while maintaining good ion selectivity. The additional membranes prepared with alternating sequence of polycations recorded significantly different water permeabilities; (A) values of 3.4 and 10.1 L m^{-2} h^{-1} bar^{-1} for Pan-PEI-PAH and Pan-PAH-PEI, respectively. The commercial nanofiltration membrane (NF 90) recorded an A value of 8.9 L m^{-2} h^{-1} bar^{-1} which was similar to that of the best performing layered membrane.

The MgSO$_4$ salt was highly rejected by all members, and 97% was the maximum rejection value recorded for the Pan-PAH_3 membrane (Fig. 9). The order of removal was as follows: MgSO$_4$ > CaCl$_2$ > NaCl ≥ KCl for all the membranes types. The estimated hydrated radii for the tested cations ranged from 0.6 to 3 nm and the pore size of NF membranes ranges from 1 to 10 nm [7,44]. Therefore, membrane sieving effect or size exclusion was not the only ion retention mechanism. But other dominant forces (i.e., electrostatic and acid-base interaction forces) were responsible for the selective removal of the salts in the feed stream. Worth noting is that ion rejection was dependent on permeability rate, that is; most of the membranes with low A values had significantly high ion rejection. As the surface forces are stronger than the drag forces for low pressures, the solute flux is less than solvent flux due to surface forces, and rejection rate (which is the ratio of the solute flux to the solvent flux) increases. However, when the drag force becomes higher the effect of surface forces becomes more and more negligible, and the solute flux increases. Therefore, if the difference between the solute and solvent fluxes decreases, then the rejection rate reduces [4,5,8,45]. From each set of prepared membranes,
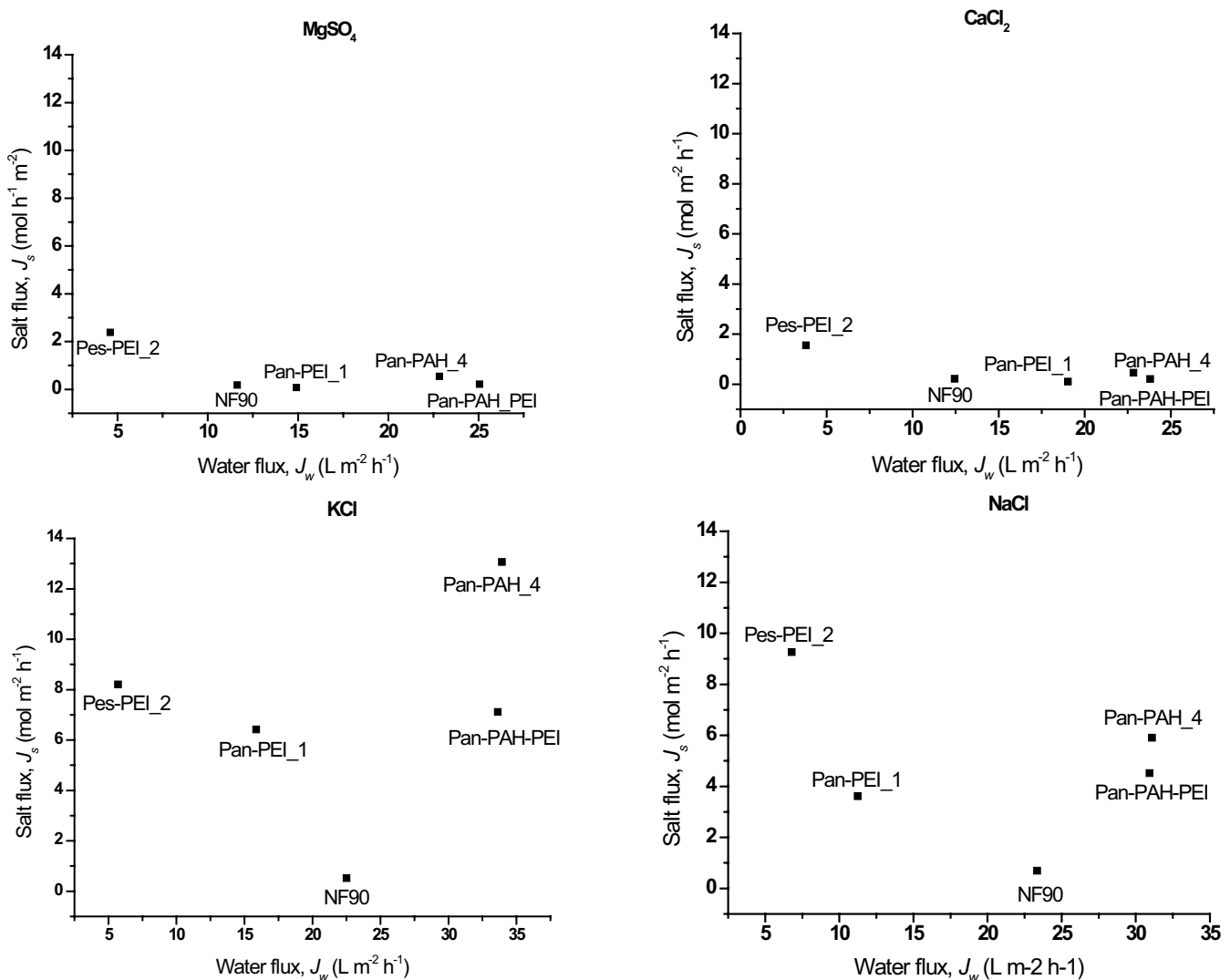

Fig. 10. Salt and water fluxes for the tested mineral salts for the best performing membranes.

there was one outstanding type that attained good water permeability and solute rejection.

3.4.2. Salt transport

The passage of salts through the membrane was calculated for all membranes by computing the B (solute permeability coefficient) and J_s (Salt flux) values using Eqs. (6) and (8). However; only the data for the best performing membrane based on permeate flux and salt rejection in each set is presented in Table 5. These performance indicators were compared with that of the high salt rejecting commercial NF90 membrane. The B/A ratio is an important selectivity parameter in membrane-based filtration systems, and it is directly related to the reverse solute transport. A lower B/A ratio (higher selectivity) is generally preferred for enhanced solute rejection, reduced fouling tendency and more stable filtration process. The values in Table 5 reveal that the prepared membranes had a good selectivity for salt of divalent cations (low B/A ratio) at relatively good flux which correlates to the low salt flux (Fig. 10). The good solute retention decreased significantly when the membranes were tested using salts of monovalent ions. The salt permeability coefficient increased by 18–83 folds which correlates to the increase in salt flux as depicted by Fig. 10. Solutions of KCl had the highest salt flux which corroborates the poor rejection data discussed in the preceding section.

Fig. 10 further revealed that the Pan-PAH_4 and Pan-PAH-PEI membranes had the best performance amongst the prepared membranes recording an average permeate flux of 24 L m^{-2} h^{-1} with more than 80% rejection of Ca^{2+} and Mg^{2+}. The permeate flux almost doubled (from 12 to 22 L m^{-2} h^{-1}) for the NF90 membrane when rejection tests were performed with solutions of KCl and NaCl. But still had a better retention of the monovalent salts compared with the prepared membranes, which implies that the membrane was more susceptible to concentration polarization compared with the prepared LBL membranes which had constant water flux for all test solutions [46,47]. The graphs in Fig. 10 also reinforces that the ability of a membrane to retain solutes is strongly linked to permeate flux. The NF90 membrane had a better overall ion removal for all test solutions but lower permeate flux compared with the Pan-PAH_4 and Pan-PAH-PEI membranes. It can be concluded that the presence of PAH polycation on Pan-based membranes resulted in improved membrane performance. These membranes are better suited for the purpose of brackish water treatment where total removal of ions is not a necessity. The separation properties of the layered membranes can be easily tuned by selecting an appropriate number of polyelectrolyte layers for optimal filtration performance (brackish water treatment).

3.4.3. Removal discussions

The solutes used in this work are all mineral salts, which ionizes in aqueous media and are susceptible to electrostatic interactions. And the prepared membranes are hydrophilic which means they are prone to be hydrated and ionized in aqueous solutions containing electrolytes, particularly because they bear (zwitterions) amine and carboxyl groups [48,49]. To study the effects of ion adsorption in the stern plane, the zeta potential of selected good membranes was then determined using the rejection test solutions which had a fixed concentration of 30 mM and the results are listed in Table 6. The surface charges for Pan-PEI_1 and Pan-PAH-PEI were reduced by 7 and 11 mV, respectively, when zeta potential was determined using the MgSO$_4$ electrolyte solution. Whilst, there was a surface charge reversal for the Pes-PEI_2 membrane from –4.01 to +10.6 mV and a slight increase

Table 6
Membrane surface charges after testing with 30 mM of inorganic salts

Membrane	Zeta potential (mV)		
	MgSO$_4$	CaCl$_2$	NaCl
Pan-PEI_1	10.0 ± 1.1	–3.8 ± 0.9	–7.9 ± 2.5
Pes-PEI_2	10.6 ± 2.9	–21.7 ± 0.7	–2.5 ± 0.3
Pan-PAH_4	7.1 ± 0.3	–3.8 ± 0.4	–4.5 ± 0.6
Pan-PAH-PEI	3.6 ± 1.5	1.6 ± 0.7	–3.9 ± 0.7

Table 5
Calculated salt permeability coefficients for selected high performing membranes

	Salt permeability coefficient	Salts			
		MgSO$_4$	CaCl$_2$	KCl	NaCl
Pan-PEI_1	B (L m^{-2} h^{-1})	1.5 ± 0.5	2.5 ± 0.2	76.6 ± 2.3	69.5 ± 3.1
	B/A (bar)	0.2 ± 0.03	0.4 ± 0.01	12.6 ± 1.9	11.4 ± 0.1
Pes-PEI_2	B (L m^{-2} h^{-1})	25.5 ± 3.2	42.3 ± 2.2	61.1 ± 5.6	56.8 ± 1.8
	B/A (bar)	12.1 ± 1.2	20.1 ± 1.5	29.4 ± 3.2	27.0 ± 2.4
Pan-PAH_4	B (L m^{-2} h^{-1})	11.7 ± 0.5	6.5 ± 0.8	49.7 ± 3.3	63.4 ± 5.3
	B/A (bar)	1.2 ± 0.1	0.7 ± 0.03	5.0 ± 0.6	6.4 ± 0.1
Pan-PAH-PEI	B (L m^{-2} h^{-1})	4.3 ± 0.7	14.9 ± 1.3	64.5 ± 4.7	72.9 ± 0.5
	B/A (bar)	0.4 ± 0.04	1.5 ± 0.2	10.4 ± 0.2	7.2 ± 0.5
NF 90	B (L m^{-2} h^{-1})	6.7 ± 0.1	11.1 ± 1.4	10.1 ± 0.1	13.0 ± 1.2
	B/A (bar)	0.8±0.04	1.3 ± 0.05	1.1 ± 0.2	1.4 ± 0.08

for the Pan-PAH_4 membrane from +1.11 to +7.1 mV. This observation implies that the initially positive charged membranes selectively adsorbed the SO_4^{2-} and the cation (Mg^{2+}) preferentially adsorbed the negative and weak positively charge surfaces of Pes-PEI_2 and Pan-PAH_4. However, the deposition of the negatively charged PSS on the surfaces terminated by the cationic PEI/PAH layer reduced the surface charges. At high ionic concentrations the membrane charges were screened by the adsorption of counter ions in solution; accumulation of charges on the surface further shield the surface charge reducing electrostatic forces and improving ion transfer through the membrane [50,51]. Thus, the eventual salt removal was through the preferential attraction of anions and their increased concentration on the surface promoted the retention of divalent cations.

Electrostatic forces are one of the surface forces which contribute to reduced transfer of ions through the membrane but cannot be independently responsible for the retention of both NaCl and KCl. Thus, the partial removal of monovalent ions is attributed to acid-base interaction forces brought upon by the presence charged polyelectrolyte multilayers [52]. Our experimental results demonstrated that brackish water desalination at low pressure using nanofiltration is a possibility especially when the membrane has a good removal of multivalent ions and average retention of monovalent ions. By this action, water hardness is removed, and electrical conductivity significantly reduced making the water more conducive for domestic purposes. This type of membrane can eliminate the need to re-introduce monovalent ions into the treated water which is the case in high salt removing separation processes.

4. Conclusion

Three sets of LBL membranes were prepared using polyacrylonitrile and polyethersulfone as substrates. A maximum of four multilayers of PEI/PAH and PSS were deposited and the membranes were intended for brackish water desalination. Spectroscopic analysis with FTIR and XPS confirmed the presence of new functionalities on the membrane surface which were attributed to the functional groups of polyelectrolytes (PEI/PAH and PSS). It was revealed that the imbalance in charge densities/charge sites amongst the polyelectrolytes led to irregular association of film layers.

The presence of polyelectrolyte films resulted in favorable interactions between the membrane and water molecules which increased the polar component of the membrane's surface free energy thus increasing its hydrophilicity. The deposition of polyelectrolyte bi-layers created an extra resistance towards permeate water flow lowering the permeability of the substrates or unmodified membranes and subsequently improving the solute retention of resulting membranes. The prepared membranes exhibited a good rejection of salts of multivalent cations ($MgSO_4$ and $CaCl_2$) and average removal for NaCl and KCl. The eventual ion removal was a function of the combined actions of electrostatic and acid-base forces as well as the membrane sieving effect.

The LBL assembly technique (of polyelectrolytes) enabled the preparation of membranes that could be easily tailored towards effective removal of cationic species in water towards brackish and seawater desalination. Membranes constituting the PAH polyelectrolyte had the most promising performance in terms of both flux and ion/salt rejection. The experimental results revealed that the polyacrylonitrile polymer was better suited to produce high performing membranes (relatively good water flux and solute rejection) because it had a better interaction with the polyelectrolytes. The prepared membranes were better suited for brackish water treatment or hardness removal since there was no total removal of both di- and monovalent mineral salts which are essential in drinking water.

Acknowledgment

References

[1] R. Semiat, Energy issues in desalination process, Environ. Sci. Technol., 42 (2008) 8193–8201.
[2] B.A. Qureshi, S.M. Zubair, Exergetic analysis of a brackish water reverse osmosis desalination unit with various energy recovery systems, Energy, 93 (2015) 256–265.
[3] M. Mulder, Basic Principles of Membrane Technology, Kluwer Academic Publishers, Boston, 2003, Chapter 1.
[4] A.L. Desa, N.H.H. Hairom, L. Yong Ng, C. Yin Ng, M. Khairul, A.W. Mohammad, Industrial textile wastewater treatment via membrane photocatalytic reactor (MPR) in the presence of ZnO-PEG nanoparticles and tight ultrafiltration, J. Water Proc. Eng., 31 (2019) 100872.
[5] L.P. Raman, M. Cheryan, N. Rajagopalan, Consider nanofiltration for membrane separations, Chem. Eng. Prog., 90 (1994) 68–74.
[6] J. Han, Y.H. Cho, H. Kong, S. Han, H.B. Park, Preparation and characterization of novel acetylated cellulose ether (ACE) membranes for desalination applications, J. Membr. Sci., 428 (2013) 533–545.
[7] A.J. Schafer, A.G. Fane, Nanofiltration – Principles and Applications, Elsevier, New York, 2005, Chapter 4.
[8] B.B. Vyas, P. Ray, Preparation of nanofiltration membranes and relating surface chemistry with potential and topography: application in separation and desalting of amino acids, Desalination, 362 (2015) 104–116.
[9] R. Malaisamy, M.I. Bruening, High-flux nanofiltration membranes prepared by adsorption of multilayer polyelectrolyte membranes on polymeric supports, Langmuir, 21 (2005) 10587–10592.
[10] J. Saqib, A.A. Aljundi, Membrane fouling and modification using surface treatment and layer-by-layer assembly of polyelectrolytes: State-of-the-art review, J. Water Process Eng., 11 (2016) 68–87.
[11] Y.N. Yip, A. Tiraferri, W.A. Phillip, J.D. Schiffman, M. Elimelech, High performance thin-film composite forward osmosis membrane, Environ. Sci. Technol., 44 (2010) 3812–3818.
[12] L. Ouyang, R. Malaisamy, M.I. Bruening, Multilayer polyelectrolyte films as nanofiltration membranes for separating monovalent and divalent cations, J. Membr. Sci., 310 (2008) 76–84.
[13] T. Ishigami, K. Amano, A. Fujii, Y. Ohmukani, E. Kamio, T. Maruyama, M. Hideto, Fouling reduction of reverse osmosis membrane by surface modification via layer-by-layer assembly, Sep. Purif. Technol., 99 (2012) 1–7.
[14] M. Michel, D. Vautier, J.-C. Voegel, P. Schaaf, V. Ball, Layer-by-layer self-assembled polyelectrolyte multilayers with embedded phospholipid vesicles, Langmuir, 20 (2004) 4835–4839.
[15] G. Decher, J.D. Hong, J. Schmitt, Builup of ultrathin multilayer films by a self-assembly process: III. Consecutively alternating adsorption of anionic and cationic polyelectrolytes on charged surfaces, Thin Solids Films, 210 (1992) 831–835.

[16] M. Schonhoff, Layered polyelectrolyte complexes: physics of formation and molecular properties, J. Phys. Condens. Matter, 15 (2003) 1781–1808.

[17] M. Elizbieciak, M. Kolasinska, P. Warszynski, Characteristics of polyelectrolyte multilayers: the effect of polyion charge on thickness and wetting properties, J. Colloids Surfaces A: Physicochem. Eng. Aspects, 321 (2008) 258–261.

[18] M. Castelnovo, J.-F. Joanny, Formation of polyelectrolyte multilayers, Langmuir, 16 (2000) 7524–7532.

[19] S. Schwartz, J. Nigel, A. Janke, W. Jaeger, S. Pratskaya, Adsorption of polyelectrolytes with hydrophobic parts, Prog. Colloid Polym. Sci., 132 (2006) 102–109.

[20] X. Tuo, D. Chen, H. Cheng, X. Wang, Fabricating water-insoluble polyelectrolytes into multilayers with layer-by-layer self-assembly, Polym. Bull., 54 (2005) 427–433.

[21] A. Tiraferri, P. Maroni, M. Borkovec, Adsorption of poly-electrolytes to like-charged substrates induced by multivalent counter-ions as exemplified by poly(styrene sulfonate) and silica, Phys. Chem. Phys., 17 (2015) 10348–10352.

[22] R. Messina, Adsorption of oppositely charged polyelectrolytes onto a charged rod, J. Chem. Phys., 119 (2003) 8133–8139.

[23] S. Qi, C.Q. Qui, Y. Zhao, C.Y. Tang, Double-skinned forward osmosis membranes based on layer-by-layer assembly FO performance and fouling behavior, J. Membr. Sci., 405–406 (2012) 20–29.

[24] J. Su, T.-S. Chung, B.J. Helmer, J.S. de Wit, Enhanced double-skinned FO membrane with inner dense layer for wastewater treatment and macromolecules recycle using sucrose as draw solute, J. Membr. Sci., 396 (2012) 92–100.

[25] Y. Shin, J.E. Robets, M.M. Santore, The relationship between polymer/substrate charge density and charge overcompensation by adsorbed polyelectrolyte layers, J. Colloid Interface Sci., 247 (2002) 220–230.

[26] O.J. Rojas, M. Ernstsson, R.D. Neuman, P.M. Claesson, Effect of polyelectrolyte charge density on the adsorption and desorption behavior on mica, Langmuir, 18 (2002) 1604–1612.

[27] X. Lui, S. Qi, Y. Li, L. Yang, B. Cao, C.Y. Tang, Synthesis and characterization of novel antibacterial silver nanocomposite nanofiltration and forward osmosis membranes based on layer-by-layer assembly, Water Res., 47 (2013) 3081–3092.

[28] Q. Saren, C.Q. Qui, C.Y. Tang, Synthesis and characterization of Novel forward osmosis membranes based on layer-by-layer assembly, J. Environ. Sci. Technol., 45 (2011) 5201–5208.

[29] M. Hu, B. Mi, Layer-by-layer assembly of graphene oxide membranes via electrostatic interactions, J. Membr. Sci., 469 (2014) 80–87.

[30] Y. Kang, L. Emdadi, M.J. Lee, D. Lui, B. Mi, Layer-by-layer Assembly of zeolite/polyelectrolyte nano-composite membranes with high zeolite loading, J. Environ. Sci. Technol. Lett., 1 (2014) 504–509.

[31] P. Karmer, D.J. Johnson, E. Seker, N. Hilal, S.A. Altinkaya, Layer-by-layer surface modification of polyethersulfone membranes using polyelectrolytes and AgCl/TiO₂ xerogels, J. Membr. Sci., 493 (2015) 807–819.

[32] W. Choi, J. Choi, J. Bang, J.-H. Lee, Layer-by-layer assembly of graphene oxide nanosheets on polyamide membranes for durable reverse-osmosis applications, Appl. Mater. Interfaces, 5 (2013) 12510–12519.

[33] S. IIyas, J. De Grooth, K. Nijmeijer, W.M. de Mos, Multifunctional and polyelectrolyte multilayers as nanofiltration membranes and as sacrificial layers for easy membrane cleaning, J. Colloid Interface Sci., 446 (2015) 386–393.

[34] G. Zhang, H. Yan, S. Ji, Z. Lui, Self-assembly of polyelectrolyte multilayer pervaporation membranes by a dynamic layer-by-layer technique on a hydrolyzed polyacrylonitrile ultrafiltration membrane, J. Membr. Sci., 292 (2007) 1–8.

[35] G.-R. Xu, S.-H. Wang, H.-L. Zhao, S.-B. Wu, J.-M. Xu, L. Li, X.-Y. Liu, Layer-by-layer (LBL) assembly technology as promising strategy for tailoring pressure-driven desalination membranes, J. Membr. Sci., 493 (2013) 428–443.

[36] S. Qi, W. Li, Y. Zhao, N. Ma, J. Wei, T.W. Chin, C.Y. Tang, Influence of the properties of layer-by-layer active layers on forward osmosis performance, J. Membr. Sci., 423–424 (2012) 536–542.

[37] C.J. van Oss, Development and applications of the interfacial tension between water and organic or biological surfaces, J. Colloids Surf., B, 54 (2007) 2–9.

[38] C.J. van Oss, Acid-base interfacial interactions in aqueous-media, J. Colloids Surf., A, 78 (1993) 1–49.

[39] G. Wolansky, A. Marmur, Apparent contact angles on rough surfaces: the Wenzel equation revisited, J. Colloids Surf., A, 156 (1999) 381–388.

[40] J.A. Brant, A.E. Childress, Assessing short-range membrane-colloid interactions using surface energetics, J. Membr. Sci., 203 (2002) 257–273.

[41] Q. Chen, P. Yu, W. Huang, S. Yu, M. Liu, C. Gao, High-flux composite hollow fibre nanofiltration membranes fabricated through layer-by-layer deposition of oppositely charged cross-linked polyelectrolytes for dye removal, J. Membr. Sci., 492 (2015) 312–321.

[42] T. Radeva, V. Milkova, I. Petkanchin, Structure and electrical properties of polyelectrolytes multilayers formed on anisometric colloidal particles, J. Colloid Interface Sci., 244 (2001) 24–30.

[43] M.M. Motsa, B.B. Mamba, A. D'Haese, E.M.V. Hoek, A.R.D. Verliefde, Organic fouling of forward osmosis membranes: the role of feed solution chemistry and membrane structural properties, J. Membr. Sci., 460 (2014) 99–109.

[44] A.J. Schafer, A.G. Fane, Nanofiltration – Principles and Applications, Elsevier, New York, 2005, Chapter 4.

[45] L.Y. Ng, A.W. Mohammad, C.Y. Ng, C.P. Leo, R.L. Rohani, Development of nanofiltration membrane with high salt selectivity and performance stability using polyelectrolyte multilayers, Desalination, 351 (2014) 19–26.

[46] J.-Y. Lee, S. Qi, X. Lui, L. Ye, F. Hao, C.Y. Tang, Synthesis and characterization of silica gel polyacylonitrile mixed matrix forward osmosis membranes based on layer-by-layer assembly, Sep. Purif. Technol., 124 (2014) 207–216.

[47] S. Rajabzadeh, C. Lui, L. Shi, R. Wang, Preparation of low-pressure water softening hollow fibre membranes by electrolyte deposition with two bilayers, Desalination, 344 (2014) 64–70.

[48] B. Deng, J. Yin, Polymer-matrix nanocomposite membranes for water treatment, J. Membr. Sci., 479 (2015) 256–275.

[49] C. Liu, L. Shi, R. Wang, Crosslinked layer-by-layer poly-electrolyte nanofiltration hollow fibre membrane for low-pressure water softening with the presence of SO₄²⁻ in feed water, J. Membr. Sci., 486 (2015) 169–176.

[50] J.V. Nicolini, C.P. Borges, H.C. Ferraz, Selective rejection of ions and correlation with surface properties of nanofiltration membranes, Sep. Purif. Technol., 171 (2016) 238–247.

[51] O. Labban, C. Liu, T.H. Chong, J.H. Lienhard, Fundamentals of low-pressure nanofiltration: membrane characterization, modeling, and understanding the multi-ions interactions in water softening, J. Membr. Sci., 521 (2017) 18–32.

[52] P.-Y. Pontalier, A. Ismail, M. Ghoul, Mechanisms for the selective rejection of solutes in nanofiltration membranes, Sep. Purif. Technol., 12 (1997) 175–181.

Appendix A.1: UV-Vis characterization of prepared multilayered membranes

The multilayer film growth of PEI/PSS and PAH/PSS pairs on the Pan and Pes polymers was monitored using UV spectroscopy. There was significant absorbance at the region 200–400 nm, which further confirmed the deposition of polyelectrolyte multilayers. An ultraviolent-visible spectrophotometer was used to determine the membrane surface modification due to the deposition of polyelectrolytes pairs of PSS-PEI and PSS-PAH.
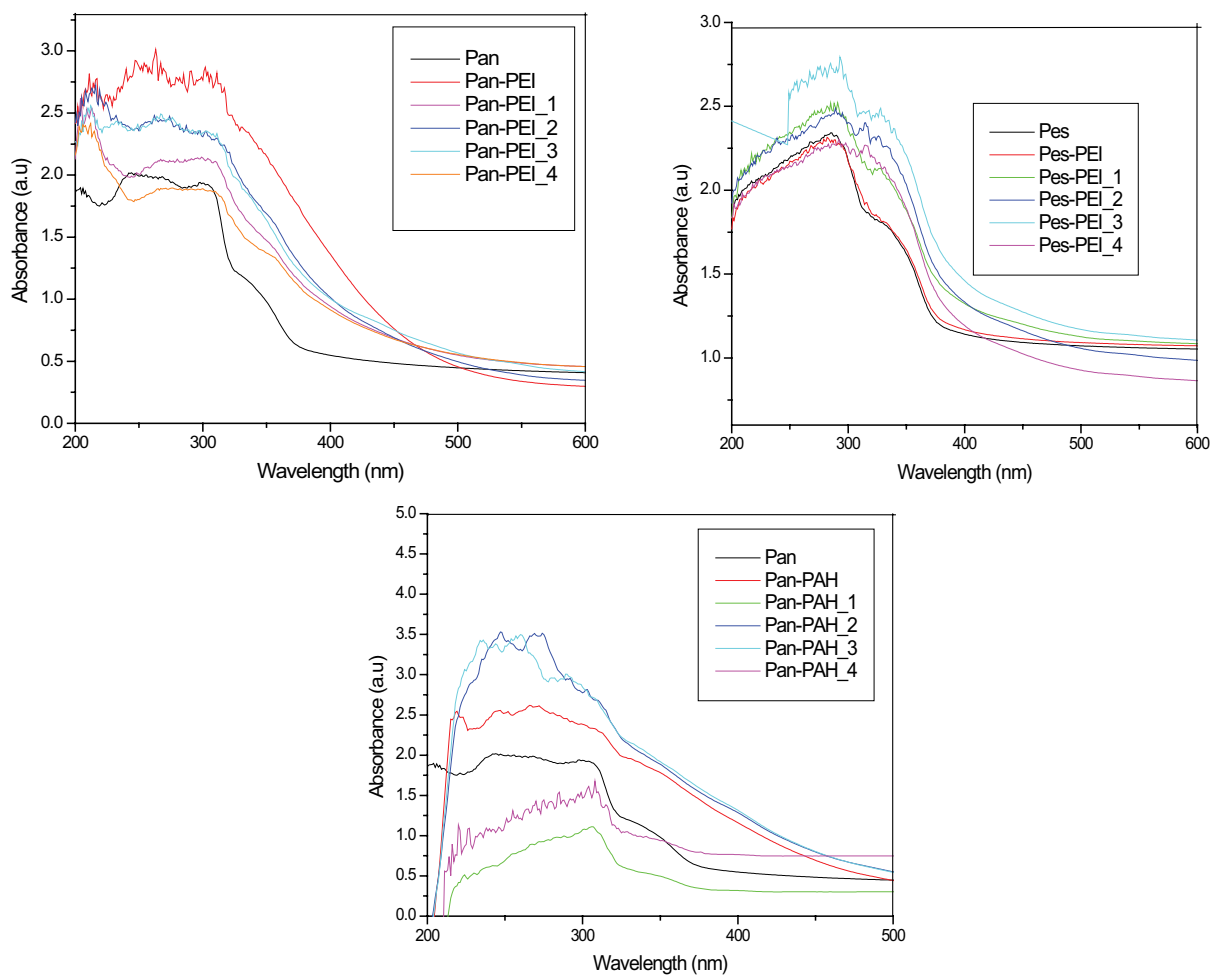

Fig. A1. (a) UV-Vis spectra of the modified membranes, (a) Pan-PEI/PSS, and (b) PES-PEI/PSS and Pan-PAH/PSS.